Fine-Crystallized LDHs Prepared with SiO_2 Sphere as Highly Active Solid Base Catalyst

Mahiro Shirotori,[a] Shun Nishimura [a,b] and Kohki Ebitani *[,a,b]

[a]School of Materials Science, Japan Advances Institute of Science and Technology, 1-1 Asahidai, Ishikawa, Nomi, 923-1292, Japan

[b]Graduate School of Advanced Science and Technology, Japan Advances Institute of Science and Technology

Author Information

Corresponding Author

K.E.: tel, +81-761-51-1610; fax, +81-761-51-1149; e-mail, ebitani@jaist.ac.jp.

Abstract

Fine-crystallized layered double hydroxides were prepared by co-precipitation method with coexistence of SiO_2 sphere (SiO_2@LDH), and these base catalysis and structural properties were investigated. As-prepared SiO_2@LDHs exhibited higher base catalysis for the Knoevenagel condensation than conventional LDHs prepared by co-precipitation method in absence of co-existence of SiO_2 sphere. Such increase in activity for base catalysis was also observed in various types of SiO_2@LDHs with different metal compositions (M^{2+}: Mg^{2+} or Ni^{2+}, M^{3+}: Al^{3+} or Ga^{3+}, M^{2+}/M^{3+}: 1 or 3). X-ray diffraction (XRD) measurement suggested that addition of SiO_2 induced the decrease in LDH crystallite size. The results of transmission electron microscopy – energy dispersive X-ray spectroscopy (TEM-EDS) and ^{29}Si cross polarization magic angle spinning nuclear magnetic resonance (^{29}Si CP-MAS NMR) on SiO_2@Mg-Al LDH suggested that the crystal of Mg-Al LDH is immobilized on SiO_2 surface through the Si-O-Al and Si-O-Mg covalent bonds. According to these results, we concluded that the co-precipitation method in the presence of colloidal spherical SiO_2 seeds, especially possessing 40 nm diameter, composed the highly-dispersed points of LDH crystal growth on SiO_2 surface, and which lead the generation of fine-crystallized highly active LDH nanocrystals.

Introduction

Layered double hydroxide (LDH) is one of well-known layered clay minerals which is composed of brucite-like two-dimensional sheets and interlayer anions. A chemical formal of LDH is generally denoted as $[M^{2+}_{1-x}M^{3+}_{x}(OH)_2]^{x+}A^{n-}_{x/n}\cdot mH_2O$, where $[M^{2+}_{1-x}M^{3+}_{x}(OH)_2]^{x+}$ corresponds to two-dimensional sheets consisting of octahedral M^{2+} and M^{3+} complex hydroxide layer. This hydroxide layer possesses positive charge derived from partially substituted M^{3+} ion. Interlayer anions A^{n-}, such as carbonate and hydroxide, and molecular water are inserted to interlayer of complex metal hydroxide layer resulting to compensate for the charge between sheets.[1-3] LDHs have been utilized

as various functional materials because of these unique characters. As examples, LDHs can be used to anions removal, drug delivery system, and preparation of nano-scale organic/inorganic hybrid materials such as bio-composite and biosensor because LDHs possess anion-exchange ability: LDHs can intercalate inorganic anions,[1, 4-5] organic anions and organic molecules.[6-8]

Additionally, the LDH materials have been widely applied as unique hydrophilic solid base catalyst for variety types of organic reactions by many researchers in the world.[9-28] The identical anions which are adsorbed onto LDH surface, such as OH^- and HCO_3^-, are known to act as base sites. As a solid base catalyst, LDH materials have some unique characteristics described as follows; (*i*) the base properties are varied in accordance with the composition of metal hydroxide and type of interlayer anions, and (*ii*) LDHs can be transformed to Lewis acidic and basic bifunctional metal composite oxide by calcination. An enormous number of studies have been devoted to investigate these utility for various organic reactions such as aldol condensation,[14, 16, 23, 25] Knoevenagel condensation,[9, 12, 15, 24] epoxidation,[10-11, 20] transesterification,[13, 17, 26] and so on. Recently, LDHs have been also utilized to advanced environmental-friendly reactions such as biomass derived saccharides conversion[18-19, 21-22, 24, 27-28] and photocatalytic conversion of CO_2 in an aqueous solution.[29-31] However, generally the anions in the interlayer space cannot participate in these chemical reactions because the high charge density of the LDHs layers and the high content of anionic species and water molecules result in strong interlayer electrostatic interactions between the sheets.[3, 32] Therefore, not only the continuous studies for applications of highly active LDH-based solid catalysts but also the improvement of preparation method to upgrade the LDH derived-solid base catalyst have been envisaged.

To overcome this issue and to upgrade the LDH derived-solid base catalyst, two strategies have been proposed; one is the delamination of LDH nanosheets, and the other is the fine-crystallization of LDH crystallite. In 2000, Adachi *et al.* reported the method of delamination of LDHs using various anionic surfactants which will lead to a novel

generation of LDH based materials in which total surface of the layered compound can be rendered accessible for chemical reactivity.[32] After that, several reports on delamination of LDHs[33-38] and method to prepare nano-hybrid materials composed of LDH nanosheets[39-43] has been presented. These methods are effective to utilize the flat plane of LDH nanosheets. Actually, various LDH nanosheets-based materials, which possess the laminated structure with other layered materials or metal nanoparticles, have been evaluated on their characteristics and utility as photo- and electro- catalysts.[39-40, 42] However, in order to improve the base catalysis of LDH itself, the delamination method seems to be insufficient, because the highly reactive sites of catalysts including LDHs are generally considered to be the edges and corners of the crystallites owing to the presence of low coordination state of atoms. As Roeffaers *et al.* reported, in the case of Li-Al LDH, transesterification occurs mainly at the {0001} plane where the basal surface of the LDH crystal, while, ester hydrolysis requires the OH^- ions at the $\{10\bar{1}0\}$ faces where the entrance of the galleries.[44] According to these previous reports, we believe that the both avoidance of *ab*-face stacking and fine-crystallization are required to maximize the base catalysis of LDH.

Immobilization of active species onto the support is one of the general methods to improve the catalytic property by avoidance of aggregation and excess growth of active species. Although the LDHs has often been used as a carrier to immobilize active species, we anticipated that the fine-crystallized LDHs can be prepared if the active LDHs can be immobilized onto the adequate carrier. To date, several nano-LDH materials which possess core-shell, yolk-shell or hollow-shell structure had been demonstrated.[45-50] A typical structure generally denoted as SiO_2@LDH is one of a hierarchical core-shell LDH material which promises strategy to avoid the *ab*-face stacking aggregation.[50] Two type procedures to prepare hierarchical SiO_2@LDH materials have been reported. Shen *et al.* demonstrated that core-shell, yolk-shell and hollow-shell SiO_2@LDH and SiO_2-coated Fe_3O_4 magnetite core-shell Fe_3O_4@SiO_2@LDH material can be obtained by layer-by-layer deposition process followed by *in situ* coating of AlOOH on SiO_2 (~340

nm) or Fe_3O_4@SiO_2 (~310 nm) core surface and successive growth of LDH crystals.[45-46] Using similar layer-by-layer method, Wang *et al.* prepared SiO_2@LDH nanoparticles over more small SiO_2 nanoparticles (~50 nm).[49] Another procedure is a simple method by using an *in situ* co-precipitation to directly deposit LDH precursors on the SiO_2 surface without any binder, reported by Chen *et al.*[47, 50] Advantages of Chen's reports are (*i*) the preparation method is very simple and easily handled and (*ii*) the size of SiO_2 spheres and the composition of LDH as well as the thickness of LDH layer can be controlled.

The LDH nanosheets derived materials, SiO_2@LDH nanoparticles and alkylcarboxylate-intercalated layered hydroxyl double salts, have been evaluated on their characteristics and utility as photo- and electro- catalysts,[39-40, 42] high active base catalyst for the Knoevenagel condensation[51] and epoxidation,[52] magnetic separation of proteins,[45] pseudocapacitance,[46] flame retardancy of epoxy resins[48] and adjuvant.[49] However, there are no reports on investigation of the improvement of base catalysis of LDH itself by fine-crystallization followed by *in situ* growth method of SiO_2@LDH nanoparticles.

The main subject of this research is the improvement of base catalysis of widely-used LDH material with unique strategy. Herein, we establish the small-crystallized LDH catalyst on SiO_2 nanoparticles and compare its base catalysis for the Knoevenagel condensation of benzaldehyde with conventional LDHs. A crystallite property, morphology and correlation between SiO_2 sphere and LDH were investigated by XRD, TEM-EDS and ^{29}Si CP-MAS NMR analytical methods. It is revealed that the coexistence of small SiO_2 sphere surfaces generate the starting points of LDH growth *via* Si-O-M covalent bond formation, leading to the fine-crystal LDH forming and enhancement of base catalysis for the Knoevenagel condensation.

Experimental

Materials and synthesis of catalysts

Tetraethyl orthosilicate (TEOS), triethanolamine (TEA) and benzaldehyde were purchased from Sigma-Aldrich Inc. Sodium carbonate (Na_2CO_3), sodium hydroxide (NaOH) and toluene were supplied by Kanto Chem. Co. Ltd. Cetyltrimethylammonium bromide (CTAB), aqueous solution of ammonium (25%), magnesium nitrate hexahydrate ($Mg(NO_3)_2{\cdot}6H_2O$), aluminium nitrate enneahydrate ($Al(NO_3)_3{\cdot}9H_2O$), nickel nitrate hexahydrate ($Ni(NO_3)_2{\cdot}6H_2O$), gallium nitrate *n*-hydrate ($Ga(NO_3)_3{\cdot}nH_2O$) and benzoic acid were obtained from Wako Pure Chemical Ind., Ltd. Co. Urea and ethyl cyanoacetate were purchased from Junsei Chemical Co., Ltd. and Tokyo Chemical Ind., Co., Ltd., respectively. The commercial Mg-Al(3)LDH (denoted as LDH(com.)) was obtained from Tomita Pharmaceutical Co., Ltd.

Spherical SiO_2(40nm) was prepared according to the previous reports.[49, 53] 96 mmol of TEA and 2 mL of TEOS were combined in a 200 mL of eggplant flask. The two-phase mixture was heated in an oil bath at 363 K for 20 min without stirring. When the mixture was taken out from the oil bath, 26.0 mL of an aqueous solution (2.8 wt%) of CTAB pre-heated at 333 K was immediately added as structure directing agent in a condensation process, and then continuously stirred for 24 h at room temperature. Thereafter, the resulting mixture was added in 50 mL of ethanol to obtain colloidal aqueous suspension. The obtained precipitate was centrifuged for 5 min at 4000 rpm. After decantation, the sediment was re-dispersed through vigorous stirring in 50 mL of an ethanolic solution of ammonium nitrate (20 g L^{-1}) and then refluxed for 1 h. This procedure was repeated three times. Then, the same operation was also performed with a solution of concentrated hydrochloric acid in ethanol (5 g L^{-1}) to replace the ammonium ions. The final sediment was washed with ethanol, and then dried *in vacuo*. The obtained spherical SiO_2 powder was calcined at 823 K under 1 L min^{-1} of air flow for 6 h.

Spherical SiO_2(250nm) was prepared using a modified literature method.[50] 13.5 mmol of TEOS was added to a mixed solution of 6.45 mL of ammonia (25 wt%), 23.55 mL of water and 50 mL of ethanol. The white suspension was stirred for 17 h at room temperature, and then centrifuged for 1 min at 4000 rpm. The obtained sediment was washed with ethanol, and then dried *in vacuo*. The resulting spherical SiO_2 powder was calcined at 823 K under 1 L min^{-1} of air flow for 6 h.

The SiO_2(*X*)@M^{2+}-M^{3+}(*Y*)LDH catalysts (*X*: desired size of spherical SiO_2; 40 nm or 250 nm, *Y*: M^{2+}/M^{3+} mol ratio; 1 or 3) were prepared *via* an *in situ* co-precipitation method according to a previous report.[50] Spherical SiO_2 particles with the desired size were dispersed in 20 mL of water using ultrasound treatment. After 30 min, the 0.96 mmol of Na_2CO_3 was added to the solution and a further 5 min of sonication was carried out. 19.2 mL of metal nitrates aqueous solution ($[M^{2+}] + [M^{3+}] = 0.075$ M) was slowly dropped into the above spherical SiO_2 dispersed solution under stirring at room temperature. The pH was maintained at 10.0 by an aqueous NaOH solution (1 M) during titration. The obtained suspension was stirred further 1 h. The resulting paste was filtered, washed with 1 L of water and ethanol, and then dried at 383 K overnight. The $Si/(M^{2+}+M^{3+})$ atomic ratios were basically adjusted to 0.50.

The M^{2+}-M^{3+}(3)LDH(CP) was synthesized by co-precipitation method. An aqueous solution of $M^{2+}(NO_3)_2{\cdot}mH_2O$ and $M^{3+}(NO_3)_3{\cdot}nH_2O$ ($M^{2+}/M^{3+} = 3$, $[M^{2+}] + [M^{3+}] = 0.075$ M, 19.2 mL) was slowly dropped into an aqueous Na_2CO_3 solution (0.048 M, 20 mL) with stirring at room temperature. The pH was kept to 10.0 by an aqueous NaOH solution (1 M) during titration. The obtained mixture was stirred further 1 h. The resulting paste was filtered, washed with 1 L of water and ethanol, and then dried at 383 K overnight. These LDHs are denoted as M^{2+}-M^{3+}(*Y*)LDH or LDH(CP).

The Mg-Al(3)LDH(U-CP) was prepared by urea co-precipitation method. 5.625 mmol of $Mg(NO_3)_2{\cdot}6H_2O$, 1.875 mmol of $Al(NO_3)_3{\cdot}9H_2O$ and 17.5 mmol of urea were dissolved in 500 mL of water, and then stirred at 373 K for 48 h. After cooling for 2 h, the obtained sediment was filtered, washed with 1.5 L of water and then dried at 333 K

overnight. This LDH is denoted as LDH(U-CP).

Reaction

Knoevenagel condensation of benzaldehyde with ethyl cyanoacetate was performed in a 20 mL of Shlenk tube under an N_2 flow (30 mL min^{-1}). The reaction was typically performed using 1.0 mmol of benzaldehyde, 1.2 mmol of ethyl cyanoacetate, 10 mg of catalysts and 3 mL of toluene at 313 K. The obtained products were analysed using GC-FID (SHIMADZU GC-2014) equipped with a polar column (Agilent, DB-FFAP).

Characterizations

X-ray diffraction patterns (XRD) were collected on a SmartLab (Rigaku) using Cu *K*α X-ray source (40 kV, 30 mA). The LDH (003) and (110) crystallite sizes were calculated by the Scherrer equation; $D_{hkl} = K\lambda/(\beta\cos\theta)$ (K: Scherrer number (0.9), λ: incident ray wavelength (0.1542 nm), β: peak width at half height (rad), θ: Brag angle). ^{29}Si cross polarization magic angle spinning nuclear magnetic resonance (^{29}Si CP-MAS NMR) measurements were performed on a AVANCE III 500 MHz (Bruker) in a 4 mm ZrO_2 rotor. The spinning rate was 8 kHz. The ^{29}Si chemical shifts are referenced to hexamethyl cyclotrisiloxane (taken to be at δ = -9.6875 ppm). Scanning electron microscope (SEM) images were collected on a S-4500 (Hitachi). The sample powder was fixed onto a carbon tape and pretreated with a PtPd ion-sputter (Hitachi, E-1030) to reduce charge up issue. Transmission electron microscopy (TEM) images were taken using a H-7100 (Hitachi) at 100 kV. TEM-energy dispersive X-ray spectroscopy (TEM-EDS) elemental mapping was obtained by a JEM-ARM200F (JEOL) at 200 kV. N_2 adsorption measurements were carried out to determine the BET (Brunauer-Emmett-Teller) specific surface area for spherical SiO_2. The measurements were conducted at 77 K on a BELSORP-max (BEL Japan, Inc.). Inductively coupled plasma - atomic emission spectrometry (ICP-AES) was operated on the iCAP6300Duo (Thermo Fisher Sci.) to estimate the amount of precipitated $M(OH)_x$ and SiO_2 in SiO_2@LDHs.

Results and discussion

Synthesis and base catalysis evaluation of SiO_2(40nm)@M^{2+}-M^{3+}LDHs

Preliminarily, we prepared SiO_2(40nm)@LDHs with various combinations and composition ratios of metal hydroxide (Mg-Al, Ni-Al and Mg-Ga type LDH with M^{2+}/M^{3+} ratio of 1 or 3) in order to investigate the correlation between these base catalytic activities and structural properties. The particle diameter of spherical SiO_2(40nm) was confirmed by TEM observation as about 40 nm (Fig. 1(A)). SEM images suggested that SiO_2 spheres were uniformly distributed as shown in Fig. 1(B)). N_2 adsorption-desorption isotherm of spherical SiO_2(40nm) showed type IV isotherm (Fig. S1), and its specific surface area calculated by BET-theory was 1081 m^2 g^{-1}.

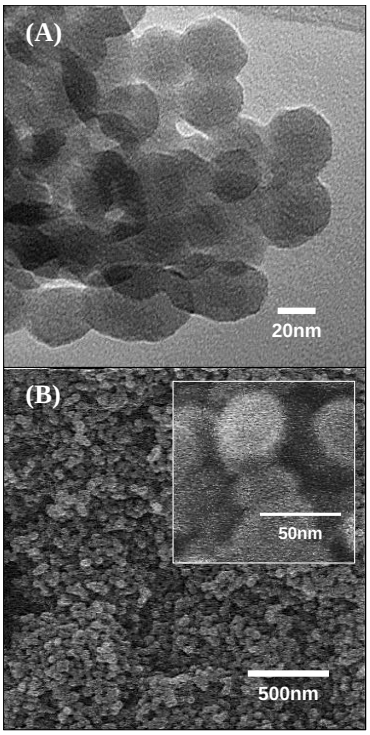

Figure 1 (A) TEM image and (B) SEM images of spherical SiO_2(40 nm).

Next, we synthesized various SiO_2(40nm)@M^{2+}-M^{3+} LDHs with M^{2+}/M^{3+} ratio of 3 by a co-precipitation with coexistence of obtained SiO_2(40nm) sphere. The actual ratios of Si/(M^{2+}+M^{3+}) and M^{2+}/M^{3+} in obtained materials were summarized in Table S1. The possibility of the residual sodium cation in the M^{2+}-M^{3+}(3) type LDHs were negligible in all M^{2+}-M^{3+}(3) type LDHs, evidenced by XPS (Fig. S2).

Fig. 2 shows time courses of benzaldehyde conversion in the Knoevenagel condensation of benzaldehyde with ethyl cyanoacetate over various M^{2+}-M^{3+}(3)LDHs and SiO_2(40nm)@M^{2+}-M^{3+}(3)LDHs. It was clearly shown that SiO_2(40nm)@M^{2+}-M^{3+}(3)LDHs efficiently mediated the Knoevenagel condensation than M^{2+}-M^{3+}(3)LDHs in all type LDHs. The reaction rates for the Knoevenagel condensation were calculated using reaction constant *k* which were estimated from the rate equation of pseudo first-order reaction, and summarized in Table 1. In the case of Mg-Al type LDH, the reaction rate for Mg-Al(3)LDH was 77 mmol g^{-1} h^{-1} whereas that of SiO_2(40nm)@Mg-Al(3)LDH was increased to 117 mmol g^{-1} h^{-1}. The increases of reaction rate by coexistence of spherical SiO_2(40nm) were more prominent in the case of Ni-Al and Mg-Ga type LDHs, and these values were respectively improved from 26 to 61 mmol g^{-1} h^{-1} and from 23 to 59 mmol g^{-1} h^{-1}. It is noted that the blank test and bare SiO_2(40nm) sphere gave no product for the Knoevenagel condensation. Thus, these results clearly indicate that co-existence of SiO_2 acts as a promoter for the base catalysis on LDHs.

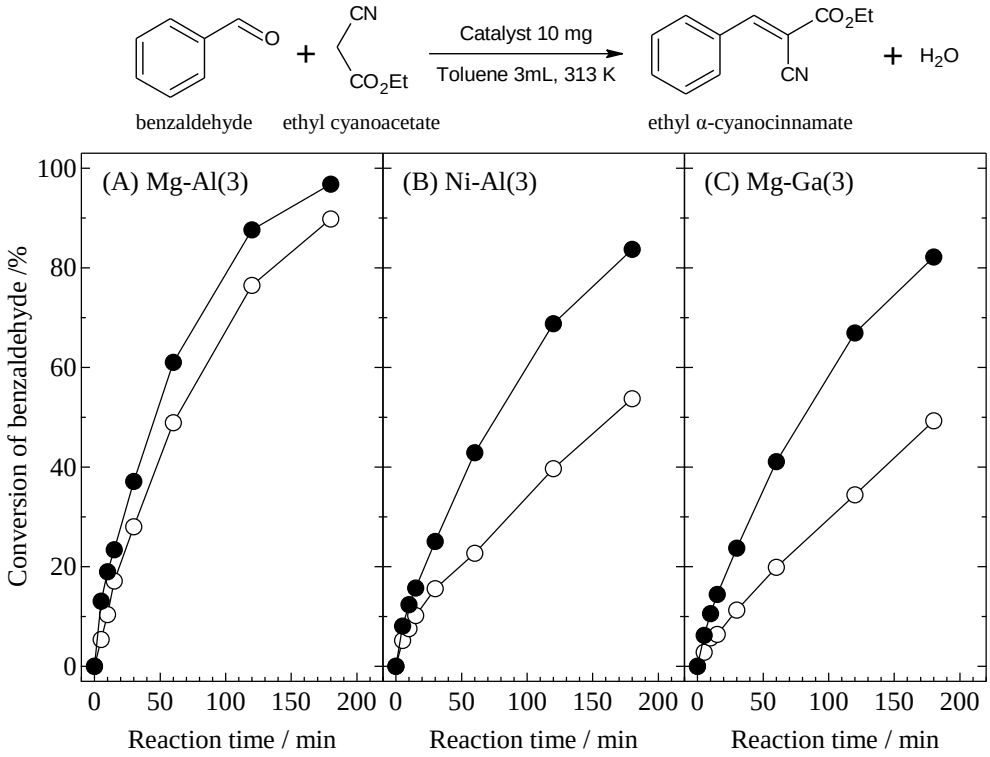

Figure 2 Activities of (○) M^{2+}-M^{3+}(3)LDH and (●) SiO_2(40nm)@ M^{2+}-M^{3+}(3)LDH with various metal compositions for the Knoevenagel condensation of benzaldehyde with ethyl cyanoacetate. *Reaction conditions*: benzaldehyde (1.0 mmol), ethyl cyanoacetate (1.2 mmol), catalyst (10 mg), toluene (3 mL), 313 K, N_2 flow (30 mL min^{-1}).

Table 1 Correlation between base activity and base property of M^{2+}-M^{3+}(3)LDHs and SiO_2(40nm)@M^{2+}-M^{3+}(3)LDHs.

Catalyst		Reaction rate[a] / mmol g^{-1} h^{-1}	Base amount[b] / mmol g^{-1}	$M(OH)_x$ amount[c] / mmol g^{-1}	Base/$M(OH)_x$[d] /%
Mg-Al(3)	LDH	76.9	0.45	12.16	3.7
	SiO_2@LDH	116.7	0.48	8.27	5.8
Ni-Al(3)	LDH	25.5	0.30	9.35	3.2
	SiO_2@LDH	60.6	0.44	7.12	6.2
Mg-Ga(3)	LDH	23.1	0.12	10.62	1.1
	SiO_2@LDH	58.8	0.37	7.52	4.9

[a]Reaction rate for the Knoevenagel condensation of benzaldehyde with ethyl cyanoacetate.

[b]Base amount calculated from poisoning test by benzoicacid titlation.

[c]Total metal M^{2+} and M^{3+} hydroxide amount calculated by ICP-AES.

[d]Base amount per total metal hydroxide amount.

Fig. 3 showed XRD patterns of various M^{2+}-M^{3+}(3)LDHs and SiO_2(40nm)@M^{2+}-M^{3+}(3)LDHs. Clear reductions in the crystalline by coexistence of spherical SiO_2(40nm) were observed in all type LDHs. Crystal properties obtained from XRD patterns are summarized in Table 2. The both crystallite sizes of stacking direction and plane direction, respectively denoted as *D*(003) and *D*(110) in SiO_2(40nm)@M^{2+}-M^{3+}(3)LDHs, were clearly smaller than those of M^{2+}-M^{3+}(3)LDHs, indicating coexistence of spherical SiO_2(40nm) inhibited the crystal growth of LDH in not only stacking direction but also plane direction. Since there were no significant change in the lattice parameter *a* and *c* between M^{2+}-M^{3+}(3)LDHs and SiO_2(40nm)@M^{2+}-M^{3+}(3)LDHs, the coexistence of spherical SiO_2(40nm) did not affect LDH unit structures. These results suggested that (*i*) coexistence of spherical SiO_2(40nm) inhibits the crystal growth of LDH, (*ii*) the obtained SiO_2(40nm)@M^{2+}-M^{3+}(3)LDHs

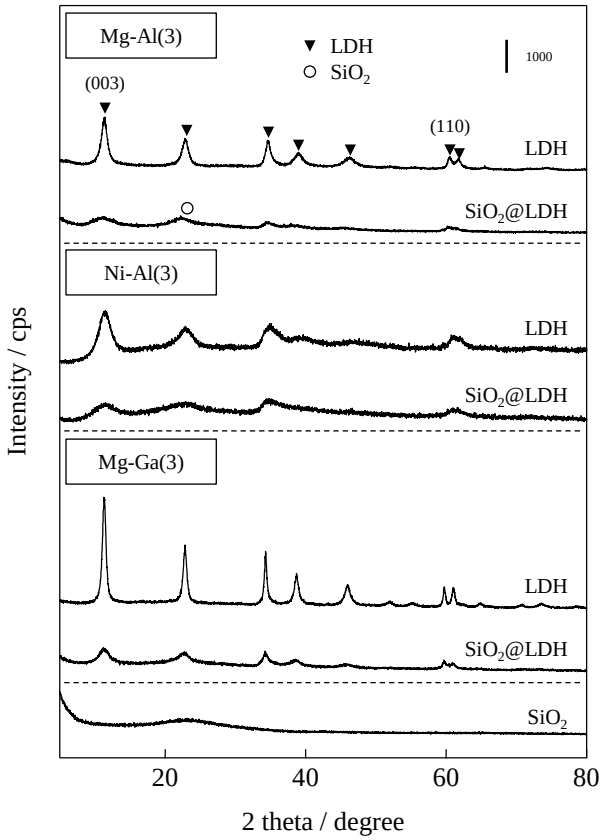

Figure 3 XRD patterns of M^{2+}-M^{3+}(3)LDHs and SiO_2(40nm)@M^{2+}-M^{3+}(3)LDHs.

possess higher activity for the basic Knoevenagel condensation than conventional M^{2+}-M^{3+}(3)LDHs, and (*iii*) those effects are similarly evolved in the cases of Mg-Al, Ni-Al and Mg-Ga type LDHs.

Table 2 Crystal properties of M^{2+}-M^{3+}(3)LDHs and SiO_2(40nm)@M^{2+}-M^{3+}(3)LDHs.

Catalyst		Lattice parameter *c* / nm	Crystallite size (003)[a] / nm	Lattice parameter *a* / nm	Crystallite size (110)[a] / nm
Mg-Al(3)	LDH	2.33	7.6	0.31	13.4
	SiO_2@LDH	2.43	2.8	0.31	8.3
Ni-Al(3)	LDH	2.31	4.0	0.30	8.1
	SiO_2@LDH	2.35	2.4	0.30	4.1
Mg-Ga(3)	LDH	2.34	13.0	0.31	24.8
	SiO_2@LDH	2.34	4.7	0.31	14.0

[a]The crystallite sizes of LDHs were calculated by Scherrer equation; $D_{hkl} = K\lambda/\beta\cos\theta$ (K: Scherrer number (0.9), λ: incident ray wavelength (0.1542 nm), β: peak width at half height (rad)).

To evaluate versatility, we prepared M^{2+}-M^{3+}(1)LDHs and SiO_2(40nm)@M^{2+}-M^{3+}(1)LDHs, and then applied these catalysts to the Knoevenagel condensation. Because base activities of M^{2+}/M^{3+} = 1 type LDHs were much lower than M^{2+}/M^{3+} = 3, the Knoevenagel condensation was carried out using substrates with half scale. As shown in Fig. S3, SiO_2(40nm)@M^{2+}-M^{3+}(1)LDHs showed higher activity than conventional M^{2+}-M^{3+}(1)LDHs in all combinations of metal hydroxides. The reaction rates were increased by coexistence of spherical SiO_2(40nm), from 7.6 to 20 mmol g^{-1} h^{-1}, from 9.6 to 29 mmol g^{-1} h^{-1} and from 15 to 20 mmol g^{-1} h^{-1} in the case of Mg-Al, Ni-Al and Mg-Ga type LDHs, respectively. Reductions in the crystalline by coexistence of spherical SiO_2(40nm) were also observed from XRD patterns as shown in Fig. S4. As same as M^{2+}-M^{3+}(3) type LDHs, the lattice parameter *c* are almost identical between M^{2+}-M^{3+}(1)LDHs and SiO_2(40nm)@M^{2+}-M^{3+}(1)LDHs whereas LDH (003) plane

crystallite sizes were reduced from 3.6 nm to 3.0 nm and from 9.7 nm to 3.4 nm in Mg-Al(1) and Mg-Ga(1) type LDHs, respectively. The reduction of crystallite size in plane direction is also observed in Mg-Al (1) and Mg-Ga(1) type LDHs whereas lattice parameter *a* does not change. The lattice parameter *c* and (003) plane crystallite size of SiO_2(40nm)@Ni-Al(1)LDH were hardly estimated because of the low intensity of diffraction peak. The lattice parameter *a* and (110) crystallite size of Ni-Al(1)LDH and SiO_2(40nm)@Ni-Al(1)LDH were also hardly estimated. These results indicated that the suppression of the crystal growth and increase of base activity were also observed in M^{2+}/M^{3+} = 1 type LDHs.

Correlation between catalytic activity and base property

Next, we investigated the correlation between base activity and basicity of M^{2+}/M^{3+} = 3 type LDHs. Base amounts were estimated by the Knoevengel condensation in the presence of benzoic acid agent: *i.e.* because the benzoic acid interfered the basic sites of LDH for the Knoevenagel condensation, the correlation between the amounts of benzoic acid and product of ethyl α-cyanocinnamate showed a linear relationship leading to the base amount. Table 1 summarizes reaction rate for the Knoevenagel condensation and base amount of LDHs. Total divalent and trivalent metal hydroxide amount ($M(OH)_x$ amount) obtained from ICP-AES and base amount per total metal hydroxide amount (Base/$M(OH)_x$) are also listed in Table 1. Compared with conventional M^{2+}-M^{3+}(3)LDHs, $M(OH)_x$ values were *ca*. 24~32% reduced in SiO_2(40nm)@M^{2+}-M^{3+}(3)LDHs because of the coexistence of spherical SiO_2(40nm). On the other hand, the Base/$M(OH)_x$ ratios were 1.6~4.5 times increased by coexistence of spherical SiO_2(40nm). This suggests that coexistence of spherical SiO_2(40nm) plays crucial role to increase the number of hydroxide layers acting as surface base sites, and it would be contributed to the enhancement in the base catalysis for the Knoevenagel condensation in the cases of SiO_2(40nm)@M^{2+}-M^{3+}(3)LDHs.[61]

The morphology and interaction between SiO_2 and LDH in SiO_2(40nm)@Mg-Al(3)LDH were investigated by TEM and ^{29}Si CP-MAS NMR

experiment. Fig. 4 showed TEM images of Mg-Al(3)LDH and SiO_2(40nm)@Mg-Al(3)LDH. The platen crystal size of SiO_2(40nm)@Mg-Al(3)LDH was smaller than that of Mg-Al(3)LDH. Besides, since SiO_2 spheres that should coexist in SiO_2(40nm)@Mg-Al(3)LDH was hardly observed in Fig. 4(B), we applied EDS elemental mapping to SiO_2(40nm)@Mg-Al(3)LDH as shown in Fig. 5. It was confirmed that Mg and Al was uniformly dispersed in wide range whereas Si was prejudiced and covered with Mg and Al to form SiO_2 core ― LDH shell like structure (Fig. 5 (A)-(E)). Same trend was observed in high magnification visual fields (Fig. 5 (F)-(J)). Moreover, the shape of SiO_2 was not spherical but shapeless. These results suggested that spherical structure of SiO_2 was crumbled in the course of catalyst preparation, and was transferred to the shapeless structure. Because it is well known that SiO_2 is dissolved in basic condition, SiO_2(40nm) spheres possessing small high specific surface area would be partially dissolved and reprecipitated in the course of LDH crystal growth method. In fact, when we treated spherical SiO_2(40nm) in basic condition (pH = 10) for 1 h at room temperature, it formed shapeless structure (Fig. S5).[62]

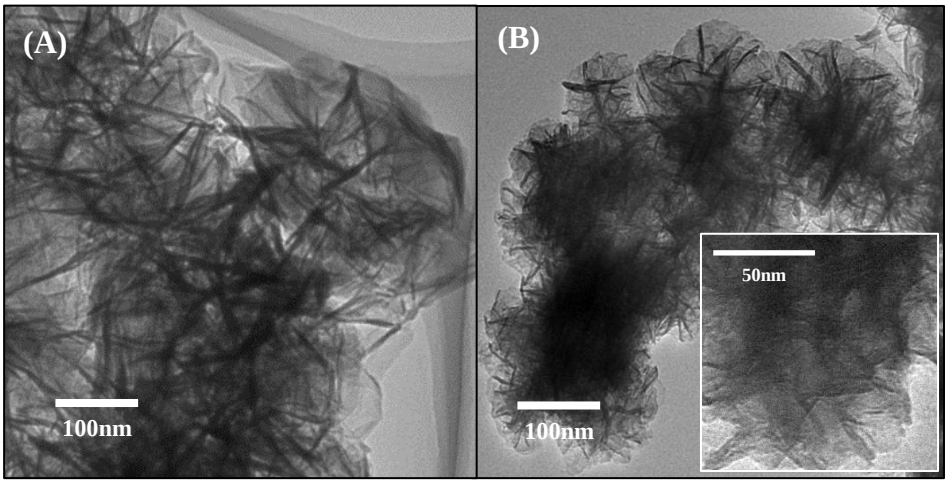

Figure 4 TEM images of (A) Mg-Al(3)LDH and (B) SiO_2(40nm)@Mg-Al(3)LDH.

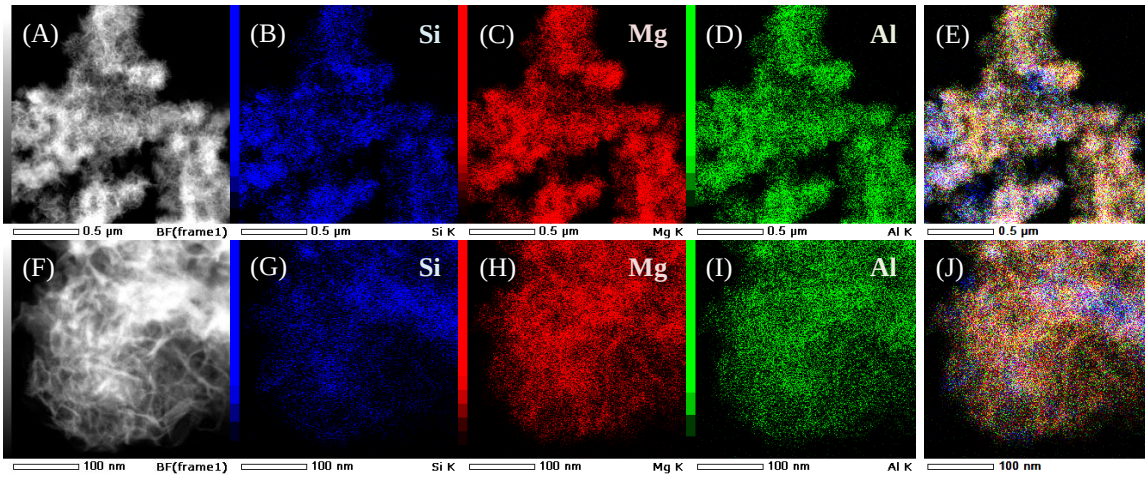

Figure 5 (A, F) Dark-field TEM images. Also shown are (B-E), (G-J) EDS mapping results of SiO_2@Mg-Al(3)LDH. (A-E): Low magnification visual field, and (F-J): high magnification visual field.

Fig. 6 shows the ^{29}Si CP-MAS NMR spectra of spherical SiO_2 and SiO_2(40nm)@Mg-Al(3)LDH. Q^n designated the Si-centered tetrahedral structural species where Q refers to silicon atom and n denotes the number of bridging oxygens. The ^{29}Si CP-MAS NMR of spherical SiO_2(40nm) showed three peeks at -91, -100, and -109 ppm which respectively correspond to Q^2, Q^3, and Q^4.[54-56] On the other hand, SiO_2(40nm)@Mg-Al(3)LDH showed a broad resonance between -70 to -115 ppm, which can be deconvoluted into four peaks centered at -78, -85, -92, and -101 ppm. The peak at -78 ppm can be assigned to Q^0 and/or Q^1 species[55] generated because of dissolution and reprecipitation of SiO_2 sphere. Reportedly, Si-centered tetrahedral structure which possess Si-O-Al and Si-O-Mg bond gave some resonances between -73 to -105 ppm[50, 57-59] and -70 to -93 ppm,[56, 60] respectively, as described in Table S2. According to previous reports, the two signals appearing at -85 and -92 ppm were assigned respectively to Si-centered compound which has Si-O-Mg and/or Si-O-Al bonds as well as overlapping with Q^2. This strongly indicates that LDH sheets and SiO_2 do not interact only by electrostatic force but also the formation of Si-O-Al and Si-O-Mg covalent bonds. According to these results, the mechanism of generation of nano-crystallized

Mg-Al LDH on SiO_2 spheres is predicted as follows: (*i*) a part of SiO_2 tetrahedral dissolves and reprecipitates (e.g. $2Q^n \leftrightarrow Q^{n+1} + Q^{n-1}$) in a basic mother solution, (*ii*) titrated Mg^{2+} and Al^{3+} ions in basic mother solution adsorb on unsaturated Si-O sites of SiO_2 surface, cause dispersion of starting points of LDH crystal growth, (*iii*) LDH nanosheets grow up from each dispersed points on SiO_2 to lead generation of small crystallite size LDH.

Evaluation of base catalysis on Mg-Al(3)LDHs with various crystalline

To evaluate the correlation between crystalline of LDH and base catalysis on LDH or SiO_2@LDH, Mg-Al(3)LDH catalysts were prepared by various methods to assess these structural properties and catalytic activities for the Knoevenagel condensation. LDH(U-CP) and SiO_2(250nm)@LDH, synthesized respectively by an urea

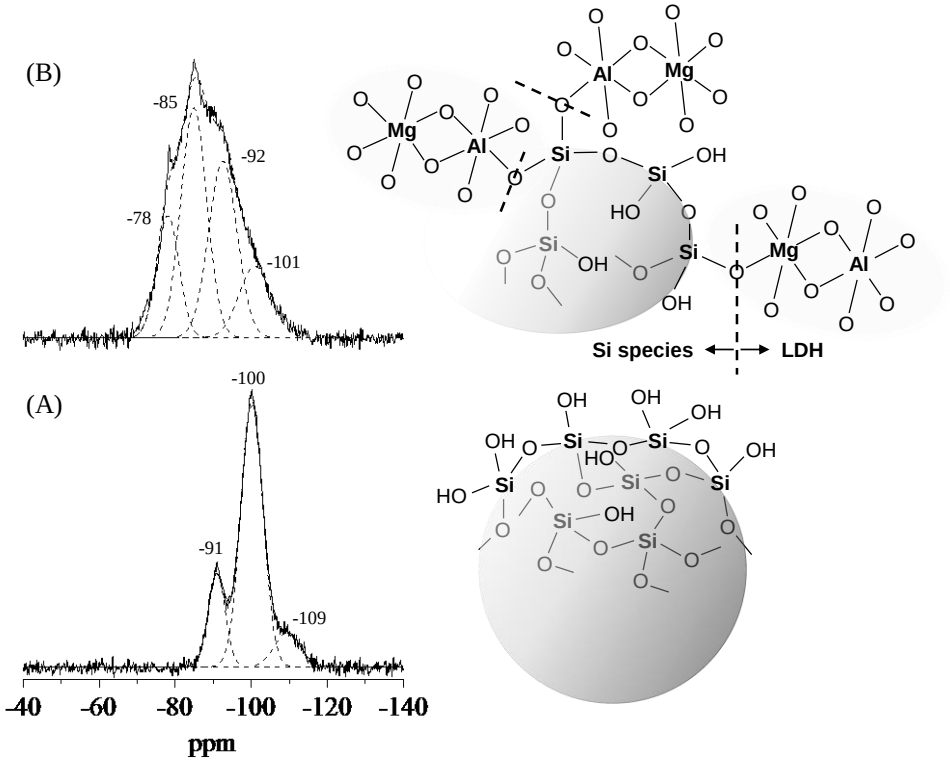

Figure 6 ^{29}Si CP-MAS NMR spectra of (A) spherical SiO_2(40nm) and (B) SiO_2(40nm)@Mg-Al(3)LDH.

co-precipitation method and an *in situ* co-precipitation method with coexisting of SiO_2(250nm) spheres, were prepared in addition to LDH(CP) and SiO_2(40nm)@LDH. LDH(com.) purchased from Tomita Pharmaceutical Co., Ltd. was also evaluated its crystalline and base catalysis as a comparison.

Fig. 7 shows TEM images of five different Mg-Al(3)LDHs. LDH(U-CP) has well crystalline hexagonal structure. Orientations of most of LDH crystals in LDH(U-CP) and LDH(com.) are face up whereas these of SiO_2@LDHs and LDH(CP) are random, indicating the *ab*-face crystal sizes of LDH(U-CP) and LDH(com.) are bigger than LDH(CP). Moreover, the observed crystal size of SiO_2(40nm)@LDH was clearly smaller than that of SiO_2(250nm)@LDH, LDH(CP), and LDH(U-CP). SiO_2(250nm)@LDH possess a defined core-shell structure as well as result reported by Chen,[50] and its LDH crystal size was similar to that of LDH(CP).

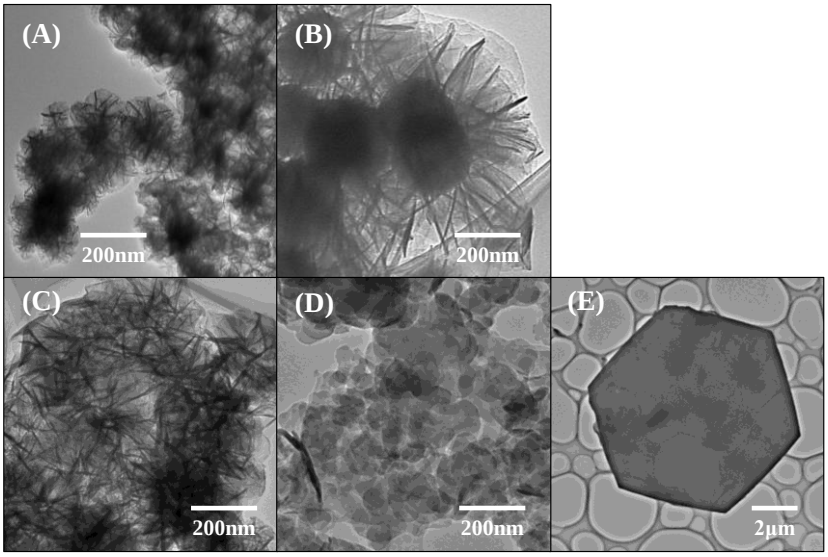

Figure 7 TEM image of various Mg-Al(3) type LDHs. (A)SiO_2(40nm)@LDH, (B) SiO_2(250nm)@LDH, (C) LDH(CP), (D) LDH(com.) and (E) LDH(U-CP).

Fig. 8 shows XRD patterns of various Mg-Al(3)LDHs. Lattice parameters and LDH (003) or (110) crystallite sizes are listed in Table 3. Similar diffraction patterns and lattice parameters were observed in all samples, indicating those LDHs composed of same LDH unit.

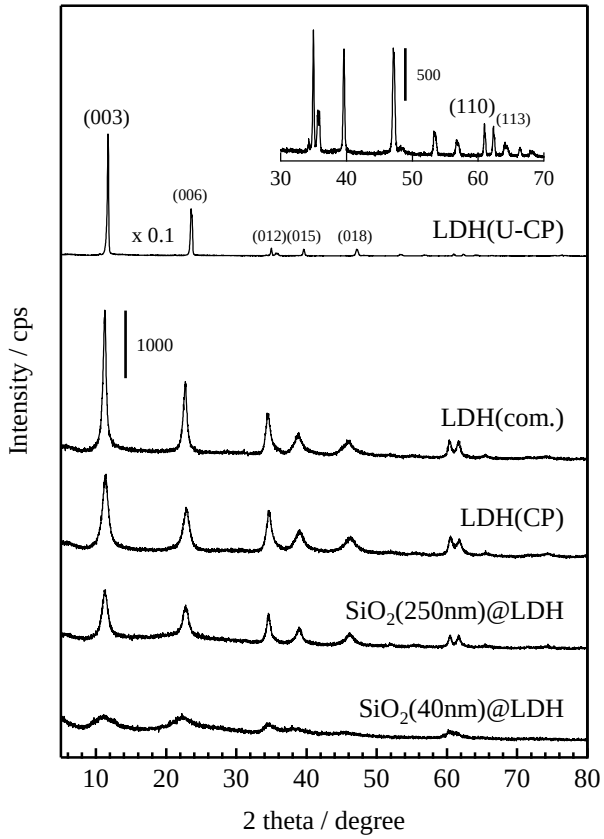

Figure 8 XRD patterns of various Mg-Al(3) type LDHs.

Table 3 Crystal properties of various Mg-Al(3)LDHs.

Type of Mg-Al(3)LDH	Lattice parameter *c* / nm	Crystallite size (003)[a] / nm	Lattice parameter *a* / nm	Crystallite size (110)[a] / nm
SiO_2(40nm)@LDH	2.43	2.8	0.31	8.3
SiO_2(250nm)@LDH	2.35	7.9	0.31	20.0
LDH(CP)	2.33	7.6	0.31	13.4
LDH(com.)	2.36	14.8	0.31	18.4
LDH(U-CP)	2.26	37.8	0.30	49.6

[a]The crystallite sizes of LDHs were calculated by Scherrer equation; $D_{hkl} = K\lambda/\beta\cos\theta$ (K: Scherrer number (0.9), λ: incident ray wavelength (0.1542 nm), β: peak width at half height (rad)).

The crystallite sizes of LDH(U-CP) and LDH(com.) were bigger than SiO_2@LDHs and LDH(CP), as expected by TEM images. Interestingly, crystallite size of SiO_2(40nm)@LDH was smaller than LDH(CP) whereas that of SiO_2(250nm)@LDH was little bigger than LDH(CP), indicating coexistence of spherical SiO_2(250nm) is not suitable for fine-crystallization of LDH. Fig 9(A) shows ^{29}Si CP-MAS NMR spectra of SiO_2(250nm) sphere. Although the broad peak between -80 to -120 ppm could be deconvoluted into three peaks centered at -92, -101, and -110 ppm as well as SiO_2(40nm) sphere, ratios of these peaks in SiO_2(40nm) sphere and SiO_2(250nm) sphere were different as shown in Table S3; the ratio for Q^4, assigned to bridging saturation silicon, in SiO_2(250nm) sphere (25%) was higher than SiO_2(40nm) sphere (11%) whereas ratios for unsaturated silicon Q^3 and Q^2 in SiO_2(250nm) sphere was lower than SiO_2(40nm) sphere. Moreover, S_{BET} of SiO_2(250nm) sphere (50 m^2 g^{-1}) was much lower than SiO_2(40nm) sphere (1081 m^2 g^{-1}). These indicate that the surface of SiO_2(40nm) sphere possess more adsorption sites for Mg^{2+} and Al^{3+} ions than

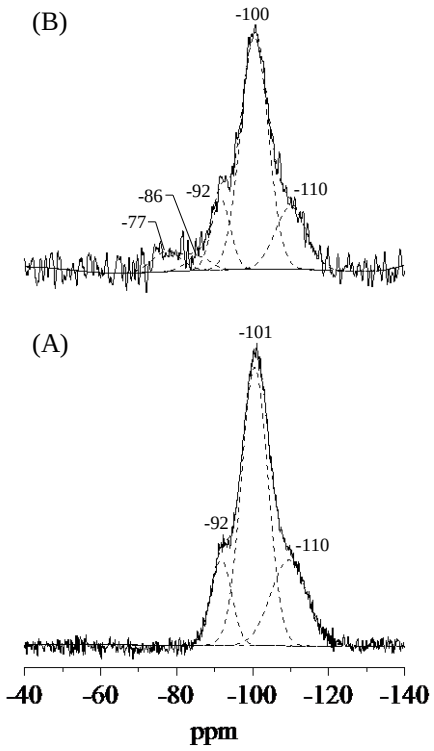

Figure 9 ^{29}Si CP-MAS NMR spectra of (A) spherical SiO_2(250nm) and (B) SiO_2(250nm)@Mg-Al(3)LDH.

SiO_2(250nm) sphere. In fact, the ratio for ^{29}Si CP-MAS NMR peak in SiO_2(250nm)@LDH (Fig. 9(B)), the degree of interactions between the SiO_2 and the LDH crystal, was only ≤ 16% whereas that of SiO_2(40nm)@LDH was ≤ 68%. These results strongly suggest that the size and surface area of spherical SiO_2 are the crucial factors to generate a small crystallite size LDH because a small spherical SiO_2 which possess high surface area can be expected to be in contact with Mg^{2+} and Al^{3+} ions, leading to enhance the dispersion of starting points of LDH crystal growth.

Catalytic activities for the Knoevenagel condensation are shown in Fig. 10 as time course of benzaldehyde conversion (Fig. 10(A)) and reaction rate (Fig. 10(B)), respectively. A high crystalline LDH(U-CP) hardly showed catalytic activity. Although LDH(com.) enhanced the Knoevenagel condensation, reaction rate was only 14 mmol g^{-1} h^{-1}. Remarkably, SiO_2(40nm)@LDH showed the highest activity with reaction rate of 117 mmol g^{-1} h^{-1} as

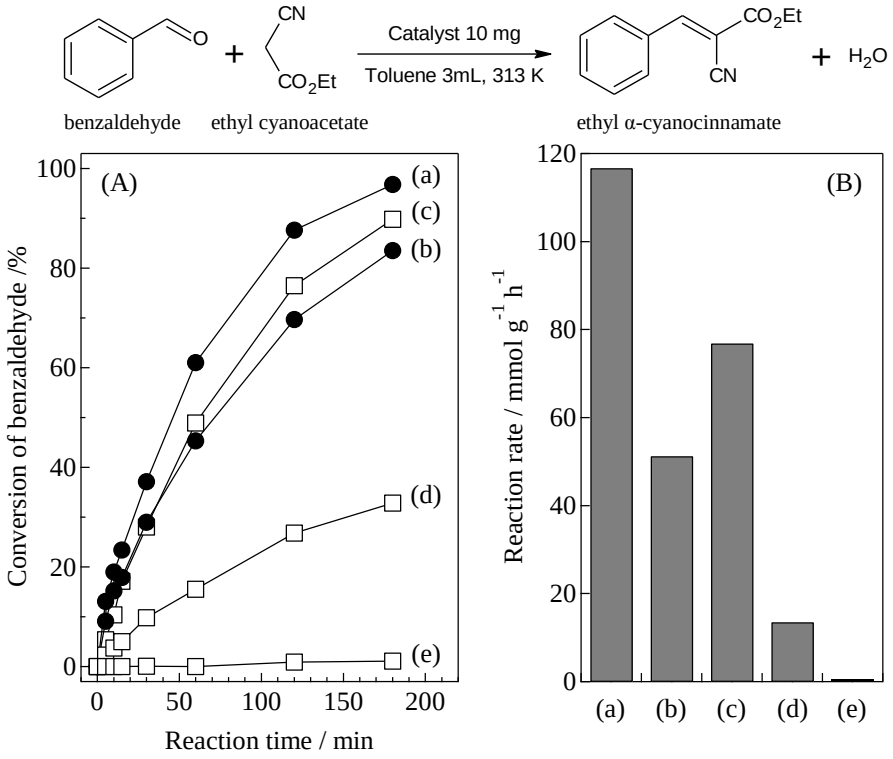

Figure 10 Activities of various Mg-Al(3) type LDHs (a) SiO_2(40nm)@LDH, (b) SiO_2(250nm)@LDH, (c) LDH(CP), (d) LDH(com.) and (e) LDH(U-CP) for the Knoevenagel condensation of benzaldehyde with ethyl cyanoacetate as (A) time cause and (B) reaction rate. *Reaction conditions*: benzaldehyde (1.0 mmol), ethyl cyanoacetate (1.2 mmol), catalyst (10 mg), toluene (3 mL), 313 K, N_2 flow (30 mL min^{-1}).

previously described. Although SiO_2(250nm)@LDH resulted reaction rate of 60 mmol g^{-1} h^{-1}, its activity was little lower than LDH(CP) (77 mmol g^{-1} h^{-1}). This strongly suggests that catalytic activity is affected by not only morphologies of LDH catalysts (*ex.* SiO_2 core – LDH shell structure) but also LDH crystallite size. On the basis of ICP-AES results, we calculated the amount of LDH structure (wt%) in the various Mg-Al(3)LDHs as shown in Table S4. The reaction rate per each LDH structure was also plotted with both LDH(003) and LDH(110) crystallite sizes in Fig.S7. These data clearly showed that the catalytic activity of obtained LDH is drastically changed by the crystallite sizes, and this tendency became significant especially below crystallite sizes of 20 nm; the catalytic activity of LDH increased with decreasing of crystallite sizes. These results support that the fine-crystallization of LDH crystallite is a crucial factor to increase the base catalysis of LDH materials.

Base amounts and apparent TOF of each base sites (TOF_{base}) in various Mg-Al(3)LDHs are listed in Table 4. Base amount of SiO_2(250nm)@LDH estimated to 0.29 mmol g^{-1} is little lower than LDH(CP) whereas apparent TOF_{base} of both SiO_2(250nm)@LDH and LDH(CP) are similar. Because crystallite of SiO_2(250nm)@LDH is similar to that of LDH(CP), it is suggested that coexistence of SiO_2(250nm) results to just immobilize LDH crystal onto SiO_2 surface without avoiding the *ab*-face stacking, so that reaction rate was smaller than LDH(CP) whereas TOF_{base} was not changed. On the other hand, SiO_2(40nm)@LDH showed higher base amount and apparent TOF_{base} than LDH(CP), indicating effects of coexistence of SiO_2(40nm) is not only

Table 4 Correlation between base activity and base property of various Mg-Al(3)LDHs.

Type of Mg-Al(3)LDH	Reaction rate[a] / mmol g^{-1} h^{-1}	Base amount[b] / mmol g^{-1}	TOF_{base} / h^{-1}
(a) SiO_2(40nm)@LDH	116.7	0.48	243
(b) SiO_2(250nm)@LDH	59.5	0.29	205
(c) LDH(CP)	76.9	0.45	171
(d) LDH(com.)	13.6	0.13	105
(e) LDH(U-CP)	0.5	n.d.	n.d.

[a]Reaction rate for the Knoevenagel condensation of benzaldehyde with ethyl cyanoacetate.
[b]Base amount calculated from poisoning test by benzoicacid titlation.

increase total base amount of LDH where the exchanged OH^- ions at the entrance of the galleries but also increase ratio of higher active site on LDH surface by fine-crystallization.

Conclusions

Highly active SiO_2(40nm)@LDH catalysts were synthesized by co-precipitation method with coexistence of small SiO_2 sphere whose particle size of *ca.* 40 nm. The results of XRD suggested that the crystallite sizes of SiO_2(40nm)@LDHs were smaller than conventional LDHs prepared by co-precipitation method without coexistence of SiO_2 sphere. All SiO_2(40nm)@LDHs showed higher catalytic activity for the Knoevenagel condensations of benzaldehyde with ethyl cyanoacetate than conventional LDHs regardless of metal compositions and ratios. Detailed characterizations on SiO_2(40nm)@Mg-Al(3)LDH using TEM-EDS and ^{29}Si CP-MAS NMR clearly revealed that SiO_2(40nm)@Mg-Al(3)LDH forms SiO_2 core ― LDH shell like structure with Si-O-Al and Si-O-Mg covalent bonds, indicating LDH crystal is immobilized on SiO_2 surface. Additionally, in comparison with various type of Mg-Al(3)LDHs prepared with different SiO_2 size and/or preparation method, the SiO_2(40nm)@Mg-Al(3)LDH prepared by co-precipitation method has the smallest LDH crystallite and gave the highest catalytic activity among all. Accordingly, we concluded that utilization of spherical SiO_2(40nm) seeds in co-precipitation method effectively generate the fine-crystallized LDH nanocrystal with high activity for base catalysis, because the high surface area and abundant Si-O sites derived from SiO_2 seeds gave highly-dispersed starting points of LDH crystal growth on SiO_2 surface.

In this paper, we successfully obtained highly active fine-crystallized LDHs *via* co-precipitation method with coexistence of SiO_2 sphere seeds, and improved the base catalysis of LDHs. The obtained SiO_2@LDH materials are composed of SiO_2 cores and fine-crystallized LDH shells, the former acts as a carrier for dispersion and immobilization of LDH and the latter as a highly active base catalyst. Spectroscopic studies well supported that the addition of small

SiO_2 sphere seeds was crucial factor to generate the starting growth points serving fine-crystallized LDHs as highly active solid base catalyst in accordance with our strategy. Thus, this approach based on material chemistry would open significant avenues to generate fine-crystalized LDH materials for versatile practical applications.

Associated Content

Supporting Information

The Supporting Information is available free of charge on the ACS Publications website at DOI:

Results of nitrogen sorption, XPS spectra, Knoevenagel condensation over M^{2+}-M^{3+}(1)LDHs and SiO_2(40nm)M^{2+}-M^{3+}(1)LDHs, XRD patterns, TEM images, assignments of ^{29}Si CP-MAS NMR, Amount of LDH, and Relation between crystallite size and reaction rate (PDF)

Acknowledgements

M.S. thanks financial support by a Grant-Aid from Japan Society for the Promotion of Science (JSPS) Fellows (No. 15J10050). The authors are indebted to Dr. Akio Miyasato (Center for Nano Materials and Technology, JAIST) and Dr. Koichi Higashimine (Center for Nano Materials and Technology, JAIST) for their great help with ^{29}Si CP-MAS NMR and TEM-EDS, respectively. ICP-AES analysis was supported by Yamato Environmental Analysis Co. Ltd.

References

1. S. Miyata, *Clays and Clay Minerals*, 1980, **28**, 50-56.
2. P. J. Sideris, U. G. Nielsen, Z. Gan and C. P. Grey, *Science*, 2008, **321,** 113-117.
3. S. Nishimura, A. Takagaki and K. Ebitani, *Green Chem.*, 2013, **15**, 2026-2042.
4. N. Iyi, T. Matsumoto, Y. Kaneko and K. Kitamura, *Chem. Mater.*, 2004, **16**,

2926-2932.

5. Y. F. Lung, Y. S. Sun, C. K. Lin, J. Y. Uan and H. H. Huang, *Sci. Rep.*, 2016, **6**, 32458.
6. J.-H. Choy, S.-Y. Kwak, J.-S. Park, Y.-J. Jeong and J. Portier, *J. Am. Chem. Soc.*, 1999, **121**, 1399-1400.
7. S. Aisawa, H. Hirahara, K. Ishiyama, W. Ogasawara, Y. Umetsu and E. Narita, *J. Solid State Chem.*, 2003, **174**, 342-348.
8. J. H. Lee, S. W. Rhee and D.-Y. Jung, *Chem. Mater.*, 2004, **16**, 3774-3779.
9. M. L. Kantam, B. M. Choudary, C. V. Reddy, K. K. Rao and F. Figueras, *Chem. Commun.*, 1998, 1033-1034.
10. K. Yamaguchi, K. Mori, T. Mizugaki, K. Ebitani and K. Kaneda, *J. Org. Chem.*, 2000, **65**, 6897-6903.
11. T. Honma, M. Nakajo, T. Mizugaki, K. Ebitani and K. Kaneda, *Tetrahedron Lett.*, 2002, **43**, 6229-6232.
12. M. J. Climent, A. Corma, S. Iborra, K. Epping and A. Velty, *J. Catal.*, 2004, **225**, 316-326.
13. M. Fuming, P. Zhi and L. Guangxing, *Org. Process Res. Dev.*, 2004, **8**, 372-375.
14. Z. An, W. Zhang, H. Shi and J. He, *J. Catal.*, 2006, **241**, 319-327.
15. E. Angelescu, O. D. Pavel, R. Bîrjega, R. Zăvoianu, G. Costentin and M. Che, *Appl. Catal. A.*, 2006, **308**, 13-18.
16. H. C. Greenwell, P. J. Holliman, W. Jones and B. V. Velasco, *Catal. Today*, 2006, **114**, 397-402.
17. E. Li, Z. P. Xu and V. Rudolph, *Appl. Catal. B*, 2009, **88**, 42-49.
18. M. Ohara, A. Takagaki, S. Nishimura and K. Ebitani, *Appl. Catal. A*, 2010, **383**, 149-155.
19. A. Takagaki, M. Ohara, S. Nishimura and K. Ebitani, *Chem. Lett.*, 2010, **39**, 838-840.
20. O. D. Pavel, B. Cojocaru, E. Angelescu and V. I. Pârvulescu, *Appl. Catal. A*, 2011, **403**, 83-90.
21. A. Takagaki, M. Takahashi, S. Nishimura and K. Ebitani, *ACS Catal.*, 2011, **1**, 1562-1565.
22. J. Tuteja, S. Nishimura and K. Ebitani, *Bull. Chem. Soc. Jpn.*, 2012, **85**, 275-281.
23. L. Hora, V. Kelbichová, O. Kikhtyanin, O. Bortnovskiy and D. Kubička, *Catal. Today*, 2014, **223**, 138-147.

24. M. Shirotori, S. Nishimura and K. Ebitani, *Catal. Sci. Technol.*, 2014, **4**, 971-978.

25. D.-G. Crivoi, R.-A. Miranda, E. Finocchio, J. Llorca, G. Ramis, J. E. Sueiras, A. M. Segarra and F. Medina, *Appl. Catal. A*, 2016, **519**, 116-129.

26. J. Nowicki, J. Lach, M. Organek and E. Sabura, *Appl. Catal. A*, 2016, **524**, 17-24.

27. M. Shirotori, S. Nishimura and K. Ebitani, *Chem. Lett.*, 2016, **45**, 194-196.

28. M. Shirotori, S. Nishimura and K. Ebitani, *Catal. Sci. Technol.*, 2016, **6**, 8200-8211.

29. K. Teramura, S. Iguchi, Y. Mizuno, T. Shishido and T. Tanaka, *Angew. Chem. Int. Ed.*, 2012, **51**, 8008-8011.

30. S. Iguchi, K. Teramura, S. Hosokawa and T. Tanaka, *Catal. Today*, 2015, **251**, 140-144.

31. S. Iguchi, S. Kikkawa, K. Teramura, S. Hosokawa and T. Tanaka, *Phys. Chem. Chem. Phys.*, 2016, **18**, 13811-13819.

32. M. Adachi-Pagano, C. Forano and J.-P. Besse, *Chem. Commun.*, 2000, 91-92.

33. E. Gardner, K. M. Huntoon and T. J. Pinnavaia, *Adv. Mater.*, 2001, **13**, 1263-1266.

34. S. O'Leary, D. O'Hare and G. Seeley, *Chem. Commun.*, 2002, 1506-1507.

35. T. Hibino, *Chem. Mater.*, 2004, **16**, 5482-5488.

36. W. Chen, L. Feng and B. Qu, *Chem. Mater.*, 2004, **16**, 368-370.

37. Z. Liu, R. Ma, M. Osada, N. Iyi, Y. Ebina, K. Takada and T. Sasaki, *J. Am. Chem. Soc.*, 2006, **128**, 4872-4880.

38. H. Kang, Y. Shu, Z. Li, B. Guan, S. Peng, Y. Huang and R. Liu, *Carbohydr. Polym.*, 2014, **100**, 158-165.

39. J. L. Gunjakar, T. W. Kim, H. N. Kim, I. Y. Kim and S. J. Hwang, *J. Am. Chem. Soc.*, 2011, **133**, 14998-15007.

40. J. Zhao, X. Kong, W. Shi, M. Shao, J. Han, M. Wei, D. G. Evansa and X. Duan, *J. Mater. Chem.*, 2011, **21**, 13926-13933.

41. W. Shi, R. Liang, S. Xu, Y. Wang, C. Luo, M. Darwish and S. K. Smoukov, *J. Phys. Chem. C*, 2015, **119**, 13215-13223.

42. C. Zhang, J. Zhao, L. Zhou, Z. Li, M. Shao and M. Wei, *J. Mater. Chem. A*, 2016, **4**, 11516-11523.

43. G. Zhu, Y. Long, H. Ren, Y. Zhou, L. Zhang, Z. Shi, F. K. Shehzad and H. M. Asif, *J. Phys. Chem. C*, 2016, **120**, 22549-22557.

44. M. B. Roeffaers, B. F. Sels, I. H. Uji, F. C. De Schryver, P. A. Jacobs, D. E. De Vos

and J. Hofkens, *Nature*, 2006, **439**, 572-575.

45. M. Shao, F. Ning, J. Zhao, M. Wei, D. G. Evans and X. Duan, *J. Am. Chem. Soc.*, 2012, **134**, 1071-1077.

46. M. Shao, F. Ning, Y. Zhao, J. Zhao, M. Wei, D. G. Evans and X. Duan, *Chem. Mater.*, 2012, **24**, 1192-1197.

47. C. Chen, P. Wang, T.-T. Lim, L. Liu, S. Liu and R. Xu, *J. Mater. Chem. A*, 2013, **1**, 3877-3880.

48. S. D. Jiang, Z. M. Bai, G. Tang, L. Song, A. A. Stec, T. R. Hull, Y. Hu and W. Z. Hu, *ACS Appl. Mater. Interfaces*, 2014, **6**, 14076-14086.

49. J. Wang, R. Zhu, B. Gao, B. Wu, K. Li, X. Sun, H. Liu and S. Wang, *Biomaterials*, 2014, **35**, 466-478.

50. C. Chen, R. Felton, J. C. Buffet and D. O'Hare, *Chem. Commun.*, 2015, **51**, 3462-3465.

51. T. Hara, J. Kurihara, N. Ichikuni and S. Shimazu, *Chem. Lett.*, 2010, **39**, 304-305.

52. T. Hara, J. Kurihara, N. Ichikuni and S. Shimazu, *Catal. Sci. Technol.*, 2015, **5**, 578-583.

53. J. Kobler, K. Möller and T. Bein, *ACS Nano*, 2008, **2**, 791-799.

54. P. N. Gunawidjaja, M. A. Holland, G. Mountjoy, D. M. Pickup, R. J. Newport and M. E. Smith, *Solid State Nucl. Magn. Reson.*, 2003, **23**, 88-106.

55. A. M. B. Silva, C. M. Queiroz, S. Agathopoulos, R. N. Correia, M. H. V. Fernandes and J. M. Oliveira, *J. Mol. Struct.*, 2011, **986**, 16-21.

56. M. Lewandowski, G. S. Babu, M. Vezzoli, M. D. Jones, R. E. Owen, D. Mattia, P. Plucinski, E. Mikolajska, A. Ochenduszko and D. C. Apperley, *Catal. Commun.*, 2014, **49**, 25-28.

57. E. Lippmaa, M. Magi, A. Samoson, M. Tarmak and G. Engelbardt, *J. Am. Chem. Soc.*, 1981, **103**, 4992-4996.

58. J. Sanz and J. M. Serratosa, *J. Am. Chem. Soc.*, 1984, **106**, 4790-4793.

59. P. P. Man, M. J. Peltre and D. Barthomeuf, *J. Chem. Soc., Faraday Trans.*, 1990, **86**, 1599-1602.

60. J.-B. d'Espinose de la Caillerie, M. Kermarec and O. Clause, *J. Phys. Chem.*, 1995, **99**, 17273-17281.

61. The BET specific surface area values of SiO_2(40nm)@Mg-Al(3)LDH and Mg-Al(3)LDH were 409 m^2 $g(cat)^{-1}$ and 150 m^2 $g(LDH)^{-1}$, respectively. On the basis

of Si content in SiO_2(40nm)@Mg-Al(3)LDH (12.3 wt%, ICP-AES), the specific surface area of Mg-Al(3)LDH itself prepared on SiO_2(40nm) surface tentatively calculated to be above 168 m^2 $g(LDH)^{-1}$, which was higher value than Mg-Al(3)LDH prepared without SiO_2 seeds.

62. To examine the actual morphology of SiO_2 in the SiO_2(40nm)@Mg-Al(3)LDH, SEM images after treatment with 1 M HCl dissolving the LDH layers of SiO_2(40nm)@Mg-Al(3)LDH were monitored. As shown in Fig. S6, the presence of shapeless SiO_2 cores was also observed in the present catalyst.